

Risk-Averse Model Predictive Control for Racing in Adverse Conditions

Thomas Lew¹, Marcus Greiff¹, Franck Djeumou^{1,2},
Makoto Suminaka¹, Michael Thompson¹, John Subosits¹

Abstract—Model predictive control (MPC) algorithms can be sensitive to model mismatch when used in challenging nonlinear control tasks. In particular, the performance of MPC for vehicle control at the limits of handling suffers when the underlying model overestimates the vehicle’s performance capability. In this work, we propose a risk-averse MPC framework that explicitly accounts for uncertainty over friction limits and tire parameters. Our approach leverages a sample-based approximation of an optimal control problem with a conditional value at risk (CVaR) constraint. This sample-based formulation enables planning with a set of expressive vehicle dynamics models using different tire parameters. Moreover, this formulation enables efficient numerical resolution via sequential quadratic programming and GPU parallelization. Experiments on a Lexus LC 500 show that risk-averse MPC unlocks reliable performance, while a deterministic baseline that plans using a single dynamics model may lose control of the vehicle in adverse road conditions.

I. INTRODUCTION

Expert racing drivers are able to pilot a vehicle at its performance limits by using all the available friction potential between the tires and the road. They are able to do this reliably lap after lap despite changes in the vehicle’s performance and behavior due to tire temperature, tire wear, and especially, weather conditions. However, current approaches to autonomous vehicle control struggle in such settings because they are sensitive to discrepancies between the model used for control and the true system [1]. This sensitivity motivates the design of new algorithms that can robustly leverage the full vehicle capabilities. Designing reliable control algorithms for racing may inform the future design of expert driver assistance systems by unlocking reliable responses for avoiding sudden obstacles, driving in adverse weather, and reacting quickly to challenges on the road.

Research in autonomous racing has boomed in the last decade, see [2] for a survey. State of the art control approaches to racing use model predictive control (MPC) to maximize path progress along a planning horizon while respecting constraints such as track bounds. These works use vehicle dynamics models of varying fidelity such as point mass models [3], [4], singletrack models

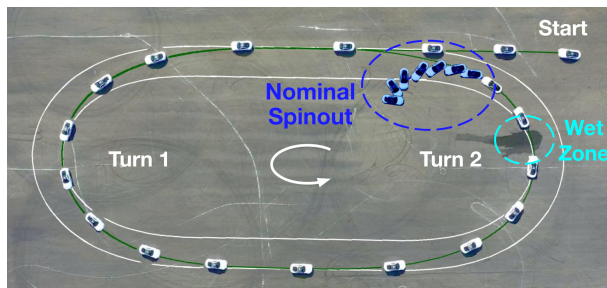


Fig. 1: Racing results through a wet area. The proposed risk-averse MPC reliably handles the vehicle throughout the turn. In contrast, a deterministic MPC controller consistently spins out the vehicle as it over-predicts the attainable tire forces.

with Pacejka [5] and Fiala tire models [6], [7], and data-driven models [8]. However, vehicle dynamics models have limitations, and although perceiving the environment to predict changes in road conditions and online adaptation can help reduce model mismatch, some factors like black ice may be difficult to observe, while reactive online learning methods may not be fast-enough to avoid leading the vehicle into an unrecoverable state.

These modeling challenges motivate the design of MPC tools that explicitly account for uncertainty to optimally trade off robustness and performance. Previous uncertainty-aware MPC methods for racing use stochastic MPC [9] and tube MPC [4]. Using a linear model of the vehicle with additive disturbances capturing model mismatch, these methods have demonstrated reliable racing performance. In [8], using Gaussian process models allowed online adaptation to gradually improve laptime. However, for computational reasons, this method fixes the uncertainty estimates during the optimization, so the MPC is not incentivized to select actions that may reduce uncertainty and lead to faster racing despite uncertainty. Also, these works use a linearization-based uncertainty propagation scheme or model uncertainties with additive disturbances that are randomized at each time, and thus neglect correlations over time. However, uncertain tire friction properties (e.g., due to driving over a wet road) may be highly correlated over time. Treating such sources of uncertain model mismatch as random disturbances may lead to suboptimal racing or to underestimating the likelihood of spinning out. As shown in [10]–[16], sample-based uncertainty-aware optimization

¹ Toyota Research Institute, Los Altos, CA, USA

² Rensselaer Polytechnic Institute, Troy, NY, USA

methods offer a potential avenue for using nonlinear dynamics models and accounting for complicated sources of uncertainties, which may necessary for expert racing.

Contributions: We introduce a risk-averse approach for racing that explicitly reasons over uncertainty:

- We propose a risk-constrained racing formulation that explicitly accounts for uncertainty over tire forces. It includes a conditional value at risk (CVaR) constraint for track bounds, nonlinear uncertain dynamics, and a cost to minimize expected lap time.
- We reformulate the risk-constrained problem using samples of the tire model parameters. Then, we propose a numerical optimization scheme that leverages the sparsity of the problem and parallelizes computations on a graphics processing unit (GPU), unlocking an uncertainty-aware MPC scheme that reasons over 10 different dynamics parameters and runs at 20Hz.

We validate the controller on a Lexus LC 500 and show that the proposed risk-constrained MPC approach unlocks reliable performance, while deterministic MPC may lose control of the vehicle in adverse conditions.

II. VEHICLE DYNAMICS AND TIRE MODEL

We use a single-track vehicle model in curvilinear coordinates [6], [17], [18], see Figure 2. We model wheelspeed dynamics to better account for wheel slippage and load transfer dynamics to account for variation in tire normal forces. We define states and control inputs

$$\begin{aligned} \tilde{x}(t) &= (r(t), v(t), \beta(t), \omega_r(t), \Delta F_z(t), e(t), \Delta\varphi(t), s(t)) \\ \tilde{u}(t) &= (\delta(t), \tau_{\text{engine}}(t), \tau_{\text{brakes},f}(t), \tau_{\text{brakes},r}(t)), \end{aligned}$$

where r is the yaw rate, v is the total velocity, β is the sideslip, ω_r is the rear wheelspeed, ΔF_z is the load transferred from the front to rear axle, e and $\Delta\varphi$ are the lateral and angle deviations to the reference trajectory, s is the progress along the reference trajectory, δ is the steering angle, $\tau_{\text{engine}} \geq 0$ is the engine torque, and $\tau_{\text{brakes},f}, \tau_{\text{brakes},r} \leq 0$ are the front and rear brake torques, respectively. We model the vehicle dynamics as

$$\begin{bmatrix} \dot{r} \\ \dot{v} \\ \dot{\beta} \\ \dot{\omega}_r \\ \dot{\Delta F}_z \\ \dot{e} \\ \dot{\Delta\varphi} \\ \dot{s} \end{bmatrix} = \begin{bmatrix} (aF_{yf} \cos \delta + aF_{xf} \sin \delta - bF_{yr})/I_z \\ (-F_{yf} \sin(\delta - \beta) + F_{xf} \cos(\delta - \beta) + F_{yr} \sin \beta + F_{xr} \cos \beta)/m \\ -r + (F_{yf} \cos(\delta - \beta) + F_{xf} \sin(\delta - \beta) + F_{yr} \cos \beta - F_{xr} \sin \beta)/(mv) \\ (\tau_{\text{engine}} + \tau_{\text{brakes},r} - F_{xr}r_w)/I_w \\ -c(\Delta F_z - \frac{h_{\text{cg}}}{a+b}(F_{xr} + F_{xf} \cos \delta - F_{yf} \sin \delta)) \\ v \sin(\Delta\varphi) \\ \dot{\beta} + \dot{r} - \kappa_{\text{ref}}v \cos(\Delta\varphi)/(1 - \kappa_{\text{ref}}e) \\ v \cos(\Delta\varphi)/(1 - \kappa_{\text{ref}}e) \end{bmatrix} \quad (1)$$

where (a, b) are the distances from the center of gravity to the front and rear axles, (I_z, m) are the vehicle inertia and mass, (r_w, I_w) are the wheel radius and the rear axle

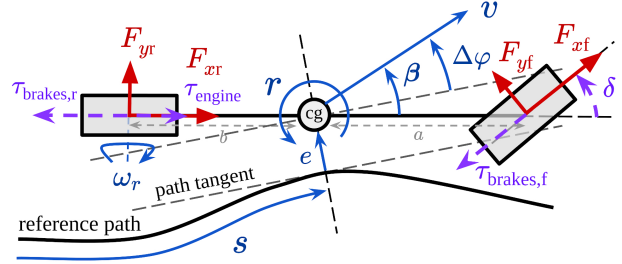


Fig. 2: Vehicle on the reference path.

inertia, $c > 0$ is a constant, h_{cg} is the center of gravity height, κ_{ref} is the curvature of the reference path.

To model tire forces $(F_{xf}, F_{yf}, F_{xr}, F_{yr})$, we use the isotropic coupled slip brush Fiala model [19], [20]

$$\begin{aligned} F_{yf} &= -F_{\text{total},f} \tan(\alpha_f)/\sigma_f, & F_{xf} &= r_w \tau_{\text{brakes},f}, \\ F_{yr} &= -F_{\text{total},r} \tan(\alpha_r)/\sigma_r, & F_{xr} &= F_{\text{total},r} \kappa_r/\sigma_r. \end{aligned}$$

The magnitude of the tire forces $(F_{\text{total},f}, F_{\text{total},r})$ are

$$F_{\text{total}} = \begin{cases} C\sigma - \frac{C^2\sigma^2}{3F_{\text{max}}} + \frac{C^3\sigma^3}{27(F_{\text{max}})^2} & \text{if } |\sigma| < \sigma_{\text{slip}} \\ F_{\text{max}} & \text{if } |\sigma| \geq \sigma_{\text{slip}} \end{cases},$$

where (σ_f, σ_r) are the total tire slips, and $(\sigma_{\text{slip},f}, \sigma_{\text{slip},r})$ are the total slips as the tires begin fully sliding

$$\sigma = \sqrt{\tan(\alpha)^2 + \kappa^2}, \quad \sigma_{\text{slip}} = \tan^{-1}(3\mu F_z/C).$$

The tire loads (F_{zf}, F_{zr}) depend on the static tire loads $(F_{\text{nom},zf}, F_{\text{nom},zr})$ as $F_{zf} = F_{\text{nom},zf} - \Delta F_z$ and $F_{zr} = F_{\text{nom},zr} + \Delta F_z$. The maximal tire forces F_{max} are

$$F_{\text{max},f} = \sqrt{(\mu F_{zf})^2 - (r_w \tau_{\text{brakes},f})^2}, \quad F_{\text{max},r} = \mu F_{zr},$$

The lateral slip angles (α_f, α_r) and longitudinal slip ratios (κ_f, κ_r) are

$$\begin{aligned} \tan(\alpha_f) &= (v \sin \beta + ar)/(v \cos \beta) - \delta, & \kappa_f &= 0, \\ \tan(\alpha_r) &= (v \sin \beta - br)/(v \cos \beta), & \kappa_r &= \frac{(r_w \omega_r - v)}{v}. \end{aligned}$$

The rear tire model explicitly computes κ_r since the rear wheelspeed ω_r is in the vehicle state. The front tire model captures coupled lateral-longitudinal tire forces by derating the F_{max} term according to the friction circle.

Many environmental factors can influence tire behavior including road conditions, tire condition, and even tire temperature [18]. With our tire model, the tire forces $(F_{xf}, F_{yf}, F_{xr}, F_{yr})$ depend on the tire-road friction μ and the tire stiffness C parameters, hereinafter defined

$$\theta = (\mu_f, \mu_r, C_f, C_r). \quad (2)$$

In Figure 3, we represent the front tire lateral forces F_{yf} as a function of the slip angle α for different values of (μ_f, C_f) . We observe that tire forces are sensitive to the choice of these parameters. Inaccurate parameter estimation may cause over-estimation of the maximum tire forces. This motivates accounting for uncertainty over these parameters to design a reliable controller.

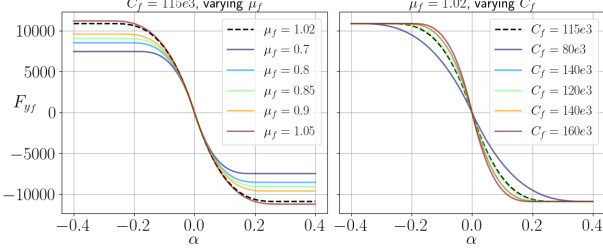


Fig. 3: Tire forces F_{yf} as a function of the slip angle α .

III. MINIMUM-TIME FORMULATION FOR RACING

Next, we describe the racing formulation used in this work. We reparameterize the state and control input as a function of path progress, add the time variable to the state, and combine the rear braking and engine torques to avoid simultaneous acceleration and braking without the need for a non-convex constraint or cost. We define

$$\begin{aligned} x(s) &= (r(s), v(s), \beta(s), \omega_r(s), \Delta F_z(s), e(s), \Delta\varphi(s), t(s)) \\ u(s) &= (\delta(s), \tau_{\text{combined},r}(s), \tau_{\text{brakes},f}(s)), \end{aligned}$$

and map the combined rear torque to the engine and rear brake torques via $\tau_{\text{engine}} = \max(0, \tau_{\text{combined},r})$ and $\tau_{\text{brakes},r} = \min(0, \tau_{\text{combined},r})$. The dynamics $x'(s) := \frac{dx(s)}{ds}$ of the resulting system are

$$x'(s) = \frac{1}{s} \left(\dot{r}, \dot{v}, \dot{\beta}, \dot{\omega}_r, \Delta \dot{F}_z, \dot{e}, \Delta \dot{\varphi}, 1 \right) (s), \quad (3)$$

where $(\dot{r}, \dot{v}, \dot{\beta}, \dot{\omega}_r, \Delta \dot{F}_z, \dot{e}, \Delta \dot{\varphi}, \dot{s})$ are given in (1).

We discretize the dynamics with a constant path progress difference $\Delta s = 3\text{ m}$ and a trapezoidal scheme

$$x_{k+1} = x_k + \frac{\Delta s}{2} (x'_k + x'_{k+1}), \quad (4)$$

where $(x_k, u_k) \approx (x(k\Delta s), u(k\Delta s))$ correspond to the state and control at $s = k\Delta s$ along the path (assuming that x_0 corresponds to $s = 0$ without loss of generality). Using a trapezoidal scheme for the dynamics constraints (4) allows us to plan with a coarse discretization Δs over large distances $N\Delta s$. We found that using explicit integrators instead (e.g., an Euler or high-order Runge Kutta schemes) can cause numerical instability if the minimum time cost dominates (see (5)). To highlight the dependency on the tire parameters $\theta = (\mu_f, \mu_r, C_f, C_r)$, the dynamics constraint (4) are equivalently written as

$$f(x_{k+1}, x_k, u_k, u_{k+1}, \theta) = 0. \quad (4)$$

The racing objective consists of minimizing lap time. To improve the robustness and smoothness of the controller, we also penalize state-control deviations to the reference $(x_{\text{ref}}, u_{\text{ref}})$ and fast changes in the control inputs. We define the linear and quadratic costs

$$\begin{aligned} \ell_T(x) &= t, \quad \ell(x, u, w) = (x - x_{\text{ref}})^\top Q(x - x_{\text{ref}}) + \\ & (u - u_{\text{ref}})^\top R(u - u_{\text{ref}}) + (u - w)^\top W(u - w) / (\Delta s^2), \end{aligned} \quad (5)$$

where (Q, R, W) are diagonal matrices with small entries compared to the terminal time cost ℓ_T . Constraints account for actuator limits (u_{\min}, u_{\max}) and ensure that the vehicle remains within the track bounds (e_{\min}, e_{\max}) . To plan over a horizon N from an initial state and control, we formulate the optimal control problem (**OCP**)

$$\begin{aligned} \min_{x,u} \quad & \ell_T(x_N) + \sum_{k=0}^{N-1} \ell(x_k, u_k, u_{k+1}) \quad \boxed{\text{OCP}} \\ \text{s.t.} \quad & f(x_{k+1}, x_k, u_k, u_{k+1}, \theta) = 0, \quad k \in [0, N-1], \\ & (x_0, u_0) = (x_{\text{init}}, u_{\text{init}}), \\ & u_{\min} \leq u_k \leq u_{\max}, \quad k \in [1, N], \\ & e_{\min,k} \leq e_k \leq e_{\max,k}, \quad k \in [1, N], \end{aligned}$$

with the notation $[0, N] := \{0, \dots, N\}$. The only non-convex term in **OCP** is the dynamics constraints.

MPC & linear interpolation: For real-time control, **OCP** is solved recursively from the current $(x_{\text{init}}, u_{\text{init}})$ and the plan (u_0, \dots, u_N) is sent to the vehicle. A low-level controller executes the control $u(s)$ at the current s via linear interpolation of the latest plan (u_0, \dots, u_N) .

IV. RISK-AVERSE FORMULATION

Solutions to **OCP** may be sensitive to the value of the tire parameters θ , and a controller that uses inaccurate values of θ may result in poor closed-loop performance. Intuitively, low friction values should result in smaller torque values to avoid spinning out or violating track bounds. In this section, we formulate a risk-averse MPC problem that accounts for uncertainty over the parameters θ distributed according to a probability distribution p_θ . First, we reformulate the track bound constraints $e_{\min,k} \leq e_k \leq e_{\max,k}$ in **OCP** as

$$g_k(x_k) := |e_k - e_{\text{mid},k}| - \Delta e_k \leq 0, \quad (6)$$

with $e_{\text{mid},k} = (e_{\max,k} + e_{\min,k})/2$ and $\Delta e_k = |e_{\max,k} - e_{\min,k}|/2$. This reformulation combines the two constraints $e_{\min,k} \leq e_k$ and $e_k \leq e_{\max,k}$ into one, simplifying the latter formulation of the risk constraint. The absolute value $|e_k - e_{\text{mid},k}|$ in (6) does not affect numerical stability, since only one of the two constraints $e_{\min,k} \leq e_k$ or $e_k \leq e_{\max,k}$ can be active at a solution.

To enforce track bound constraints and account for uncertainty over state trajectories due to uncertain tire forces, we constrain the tail probability of ever violating the constraint $g_k(x_k) \leq 0$ in (6) at any timestep k

$$\text{CVaR}_\alpha \left(\max_{k=1, \dots, N} g_k(x_k) \right) \leq 0, \quad (7)$$

where CVaR_α is the conditional value at risk at level $\alpha \in (0, 1)$ (or average value at risk [16], [21]), defined as $\text{CVaR}_\alpha(Z) = \min_{\xi \in \mathbb{R}} \mathbb{E}[\xi + \max(0, Z - \xi)/\alpha]$. Using the risk constraint (7) yields many advantages compared to other (e.g., chance-constrained) formulations, see [16].

The total cost $\ell_T(x_N) + \sum_{k=0}^{N-1} \ell(x_k, u_k, u_{k+1})$ is also a random variable as it depends on the state trajectory, so we minimize its expected (average) value, with the objective of minimizing the average lap time. We formulate the risk-averse optimal control problem (**RA-OC**P)

$$\begin{aligned} \min_{x,u} \mathbb{E} \left[\ell_T(x_N) + \sum_{k=0}^{N-1} \ell(x_k, u_k, u_{k+1}) \right] & \quad \boxed{\text{RA-OC}} \\ \text{s.t. } f(x_{k+1}, x_k, u_k, u_{k+1}, \theta) = 0, & \quad k \in [0, N-1], \\ (x_0, u_0) = (x_{\text{init}}, u_{\text{init}}), & \\ u_{\min} \leq u_k \leq u_{\max}, & \quad k \in [1, N], \\ \text{CVaR}_\alpha \left(\max_{k=1, \dots, N} g_k(x_k) \right) \leq 0. & \end{aligned}$$

RA-OCP encodes the problem of minimizing the average lap time (with additional regularization encoded by the cost term ℓ) while bounding the tail probability of leaving the track, over the uncertain parameters $\theta \sim p_\theta$.

V. SAMPLE-BASED REFORMULATION AND NUMERICAL RESOLUTION

RA-OCP is a challenging problem to solve due to the uncertainty over the parameters θ . Inspired by [16], we compute approximate solutions to **RA-OC**P by solving a sample-based reformulation instead that depends on $(1+M)$ samples θ^i of the parameters θ .

First, we select a nominal value $\bar{\theta} := \theta^0$ for the parameters θ to parameterize a nominal state and control trajectory $(\bar{x}, \bar{u}) := (x^0, u^0)$, which will be used to reduce uncertainty growth over the planning horizon via feedback. This trajectory satisfies the nominal dynamics

$$f(\bar{x}_{k+1}, \bar{x}_k, \bar{u}_k, \bar{u}_{k+1}, \bar{\theta}) = 0 \quad \forall k, \quad (\bar{x}_0, \bar{u}_0) = (x_{\text{init}}, u_{\text{init}}).$$

Second, we account for uncertainty over the parameters θ by parameterizing M state and control trajectories (x^i, u^i) around the nominal trajectory (\bar{x}, \bar{u}) . We select M samples θ^i of θ that define the state trajectories as

$$x_0^i = x_{\text{init}}, \quad f(x_{k+1}^i, x_k^i, u_k^i, u_{k+1}^i, \theta^i) = 0 \quad \forall k, \quad (8)$$

and the closed-loop control trajectories as

$$u_k^i = \bar{u}_k - K_k^i (x_k^i - \bar{x}_k) = u_k^0 - K_k^i (x_k^i - x_k^0), \quad (9)$$

where the feedback gains K_k^i are computed as the solution to a linear-quadratic regulator (LQR) problem [22, Chapter 12] around $(x_{\text{ref}}, u_{\text{ref}})$ using the parameters θ^i .

Finally, we introduce the optimization variables

$$\begin{aligned} X &= (\bar{x}, x^1, \dots, x^M) \in \mathbb{R}^{(1+M)Nn}, & \bar{u} &\in \mathbb{R}^{Nm}, \\ y &= (y^1, \dots, y^M) \in \mathbb{R}^M, & \xi &\in \mathbb{R}, \end{aligned}$$

where y and ξ are risk variables, the state and control dimensions are $(n, m) = (8, 3)$, the sample size and

horizon are $(M, N) = (10, 32)$, and formulate the following sample-based approximation to **RA-OC**P

$$\begin{aligned} \min_{x, \bar{u}, y, \xi} \frac{1}{1+M} \sum_{i=0}^M \left(\ell_T(x_N^i) + \sum_{k=0}^{N-1} \ell(x_k^i, \bar{u}_k, \bar{u}_{k+1}) \right) \\ \text{s.t. } f(x_{k+1}^i, x_k^i, u_k^i, u_{k+1}^i, \theta^i) = 0, & \quad \begin{cases} k \in [0, N-1], \\ i \in [0, M], \end{cases} \\ u_k^i = \bar{u}_k - K_k^i (x_k^i - \bar{x}_k) & \quad \begin{cases} k \in [0, N], \\ i \in [0, M], \end{cases} \\ (x_0^i, \bar{u}_0) = (x_{\text{init}}, u_{\text{init}}), & \quad i \in [0, M], \\ u_{\min} \leq \bar{u}_k \leq u_{\max}, & \quad k \in [1, N], \\ e_{\min} \leq \bar{e}_k \leq e_{\max}, & \quad k \in [1, N], \\ \begin{cases} (M\alpha)\xi + \sum_{i=1}^M y^i \leq 0 \\ 0 \leq y^i & i \in [1, M], \\ g_k(x_k^i) - \xi \leq y^i, & i \in [1, M], k \in [1, N]. \end{cases} \end{aligned}$$

Remark 1 (On closed-loop uncertainty propagation): Using a feedback law in the optimization problem **RA-OC**P to define closed-loop trajectories as in (8)-(9) is a standard approach [9], [23], [24] to prevent uncertainty to grow unbounded over time and make the optimization infeasible. It also allows approximately accounting for closed-loop feedback of the receding horizon MPC scheme. We do not enforce input constraints for the controls u^i because solutions are already constrained by the tire friction limits, although one could include closed-loop input constraints in the risk constraint (7) or saturate the controls u^i within the dynamics [25].

Efficient numerical resolution of the sample-based problem: leveraging GPU parallelization and sparsity

Efficiently solving the sample-based reformulation of **RA-OC**P requires special care due to the large size of the problem. To achieve fast replanning, we leverage two observations. First, the problem is sparse, e.g., the particle x^i does not explicitly depend on x^{i+1} . Second, since we parameterize the state trajectory x^i for each particle, the cost terms and constraints can be evaluated in parallel over both particles and time on a GPU.

Thus, we decide to solve the sample-based reformulation of **RA-OC**P via a sequential quadratic programming (SQP) method with a linesearch [26, Chapter 18]. We evaluate the cost, constraints, and their gradients in Python using Jax [27], so we can easily evaluate the quadratic programs (QPs) at each SQP step on a GPU and take advantage of the parallel structure of the sample-based reformulation. The problem data is then moved to the CPU and the QPs are solved using OSQP [28]. Even though the QPs involve many variables, they are quickly solved thanks to the sparsity of the QPs that OSQP leverages internally. For receding horizon MPC, we only perform one SQP iteration at each timestep [29].

TABLE I: Tire parameters θ^i defining **OCP** and **RA-OCP** for trajectory analysis (Sec. VI) (top) and MPC (Sec. VII) (bottom).

Trajectory Analysis		$\bar{\theta}=\theta^0$	θ^1	θ^2	θ^3	θ^4	θ^5
μ_f		1.02	0.70	0.80	0.85	0.90	1.05
μ_r		1.08	0.70	0.80	0.85	0.90	1.05
$10^{-3}C_f$		115	80	140	120	140	160
$10^{-3}C_r$		280	240	320	280	300	320

MPC	$\bar{\theta}=\theta^0$	θ^1	θ^2	θ^3	θ^4	θ^5	θ^6	θ^7	θ^8	θ^9	θ^{10}
μ_f	1.02	0.75	0.74	1.05	0.92	0.93	0.94	0.95	0.96	0.97	0.98
μ_r	1.08	0.75	0.74	1.05	0.92	0.93	0.94	0.95	0.96	0.97	0.98
$10^{-3}C_f$	115	90	130	92	125	95	121	95	110	97.5	115
$10^{-3}C_r$	280	240	320	250	300	280	290	290	310	280	290

Remark 2 (Alternatives and lessons learned): The nominal trajectory \bar{x} could be removed from the optimization variables by defining $\bar{x} = x^0 = \frac{1}{M} \sum_{i=1}^M x^i$. However, the resulting formulation densely couples the particles x^i via the feedback controls in (9) and is thus slow to solve numerically. Parameterizing the nominal trajectory greatly increases the sparsity of the problem.

We tried only optimizing over the control inputs u and computing states $x^i(u)$ for each particle via an explicit integration scheme as in [16], which we found to be numerically sensitive to the choice of initial guess. Parameterizing the particles x^i and using an implicit integrator instead improves robustness and enables parallelizing computations over times k and samples i .

VI. PROBLEM SETUP AND TRAJECTORY ANALYSIS

We consider an oval racing track shown in Figure 1. The reference trajectory $(x_{\text{ref}}, u_{\text{ref}})$ is the optimal racing line computed offline for nominal parameters $\bar{\theta}$ using the method in [6]. In this section, we study trajectories solving **OCP** and **RA-OCP** for different values of the parameters θ . For visualization purposes, we use $M = 5$ samples of the parameters, shown in Table I.

a) *How different are risk-averse solutions compared to solutions to OCP with nominal tire parameters $\bar{\theta}$?* We present trajectories solving **OCP** and **RA-OCP** in Figure 4. The risk-averse solution applies less engine torque and braking forces to account for potentially reduced tire forces (see Figure 3) and brakes earlier than the solution to **OCP**. This results in a lower velocity in the turn. We also plot closed-loop trajectories x^i satisfying (8) for **OCP** for the different parameters θ^i . The solution to **OCP** may drive too fast to complete the turn: the vehicle may slide out of the track if the tire friction parameters μ_f and μ_r take lower values. In contrast, solutions to **RA-OCP** account for different tire parameter values to ensure robust handling of the vehicle in the turn.

b) *Does solving OCP with low-friction tire parameters give robust performance?* We solve **OCP** assuming that $\theta = \theta^1$ (corresponding to low-friction tire parameters $\mu_f = \mu_r = 0.7$) and present results in Figure 5. The solution to **OCP** is now closer to the solution to

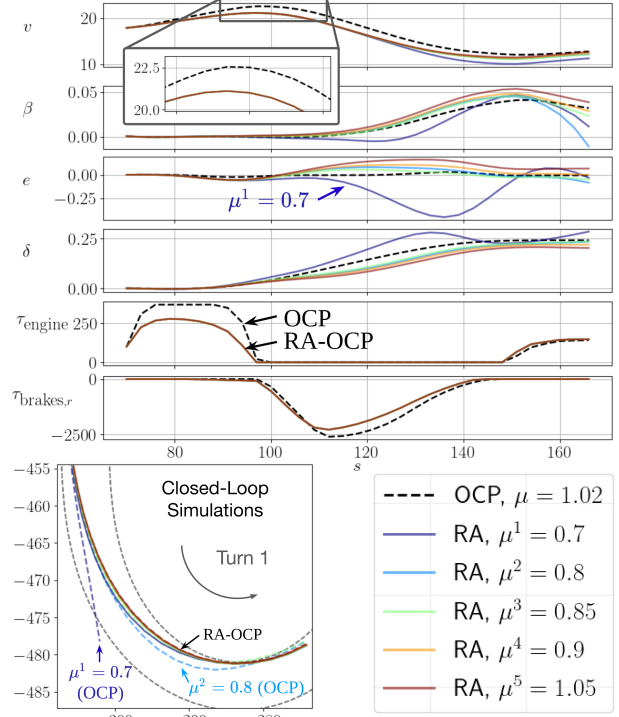


Fig. 4: Top: Nominal vs risk-averse solutions. Bottom: Closed-loop trajectories for different parameters θ corresponding to solutions to **OCP** (dashed lines) and **RA-OCP** (solid lines).

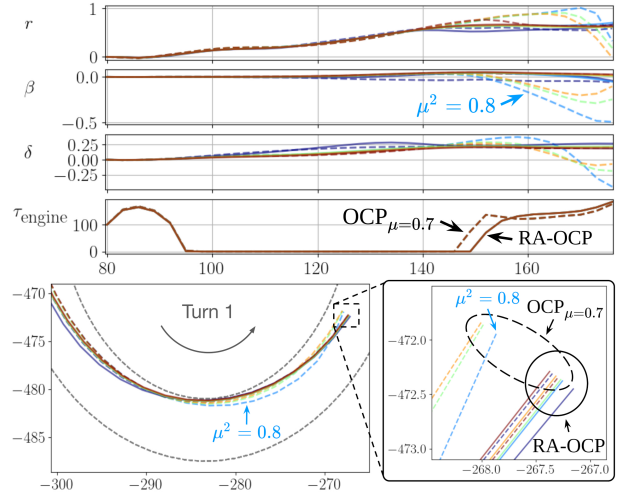


Fig. 5: Closed-loop trajectories for different parameters θ corresponding to solutions to **OCP** with low friction values $\mu_f = \mu_r = 0.7$ (dashed lines), and **RA-OCP** (solid lines).

RA-OCP and yields better performance over different tire parameter values θ^i than if assuming larger-friction tire parameters. However, the performance remains poor for different tire parameter values, e.g., exhibiting large sideslip (β) values for $\mu_f = 0.8$ that may lead to sub-optimal closed-loop performance. Overall, these results show that accounting for different tire parameters by solving **RA-OCP** gives additional robustness compared to only planning with low-friction tire parameters.

VII. HARDWARE RESULTS

We validate the risk-averse controller on a 2019 Lexus LC 500. State estimates come from an OxtS Inertial Navigation System [30]. The optimization problems are solved on an on-board computer with an Intel Xeon E-2278GE CPU @3.30GHz and an NVIDIA GeForce RTX 3070 GPU. Further details about the vehicle are in [6].

We compare the proposed risk-averse MPC approach solving **RA-OCP** with a nominal MPC solving **OCP** with the parameters $\theta = \bar{\theta}$. For all experiments, we fix the parameter samples θ^i in **OCP** and **RA-OCP** to the values in Table I to cover the parameter space. Keeping these parameter values constant in time also removes randomness in the algorithm. The nominal MPC runs at about 100Hz. The risk-averse MPC runs at 20Hz (with mean 22Hz and standard deviation 1.5Hz). These update rates are sufficient to reliably control the vehicle.

a) Racing in dry conditions: We first validate the controllers in dry conditions and report results in Figure 6. Nominal MPC (solving **OCP** with the parameters $\bar{\theta}$) applies larger engine and braking torques and drives slightly faster than risk-averse MPC (solving **RA-OCP**), with a top speed difference of 1m/s. Nominal MPC causes slight yaw rate oscillations while turning due to tire saturation. Overall, nominal MPC slightly outperforms risk-averse MPC in such dry conditions, which is expected behavior given that risk-averse MPC optimizes the expected final time over a wider range of parameters including lower friction values (μ_f, μ_r) .

We also tested nominal MPC planning with low-friction parameters $(\mu_f = \mu_r = 0.7)$. This approach consistently cuts corners in the turns due to model mismatch and is thus unable to race in dry conditions.

b) Racing through a patch of water: We test again the controllers on a dry track with a water patch in turn 2 (see Figure 1). Such conditions may represent a track that is slowly drying up after rain, resulting in a leftover patch of water. We run the controllers three times each. For repeatability, we alternate between nominal and risk-averse MPC and add water after each individual run.

Results are reported in Figure 7. After driving through the wet area when exiting turn 2, nominal MPC consistently causes a spin out, due to applying engine torques that are too large while oversteering. Indeed, tires are wet and thus cannot apply the planned tire forces, which results in a spin out. In contrast, risk-averse MPC applies slightly smaller engine torques when exiting each turn and is thus consistently able to drive through the wet area and complete the lap. While more robust behavior may be obtained with nominal MPC by reducing the minimum-time cost ℓ_T compared to the regularizer ℓ , such a strategy may require additional hyperparameter tuning and lead to suboptimality and slower lap times.

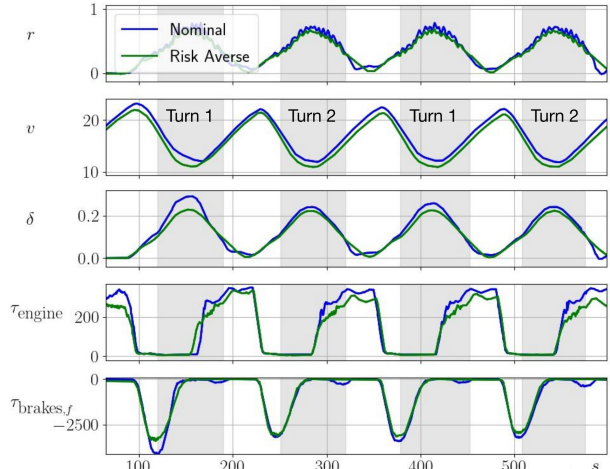


Fig. 6: Racing results in nominal dry conditions. A single run with the nominal (blue) and risk-averse MPC (green).

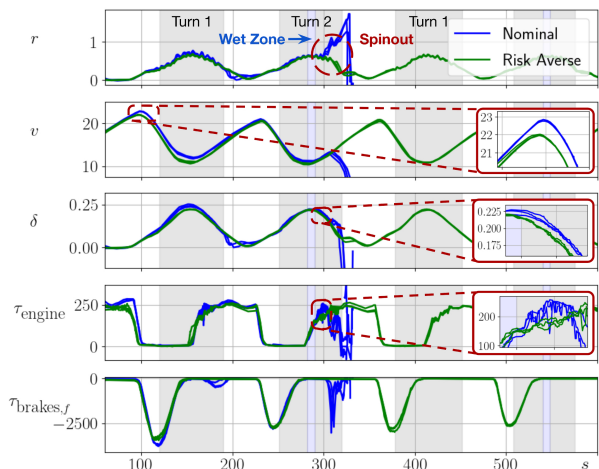


Fig. 7: Racing results with a wet area (see also Figure 1). Three runs of the nominal (blue) and risk-averse MPC (green), with close ups at peak velocity and after the wet zone in turn 2.

VIII. CONCLUSION

We presented a risk-averse MPC framework for racing and showed that accounting for different tire parameters provides a natural avenue for infusing robustness into MPC. By leveraging a particular sample-based risk-averse formulation, our method accurately accounts for uncertain nonlinear tire dynamics and is amenable to online replanning in MPC. In future work, we plan on investigating improvements to the SQP solver (e.g., by developing specialized methods inspired from [31]–[34] to solve **RA-OCP** entirely on the GPU) to unlock faster replanning and using larger sample sizes, and interfacing with perception to account for state uncertainty and parameters that vary over time and space.

ACKNOWLEDGMENTS

We thank Phung Nguyen, Steven Goldine, and William Kettle for their support with the test platform and experiments, and Jenna Lee for helping with data visualization.

REFERENCES

- [1] T. P. Weber and J. C. Gerdes, "Modeling and control for dynamic drifting trajectories," *IEEE Transactions on Intelligent Vehicles*, 2023.
- [2] J. Betz, H. Zheng, A. Liniger, U. Rosolia, P. Karle, M. Behl, V. Krovi, and R. Mangharam, "Autonomous vehicles on the edge: A survey on autonomous vehicle racing," *IEEE Open Journal of Intelligent Transportation Systems*, vol. 3, pp. 458–488, 2022.
- [3] J. K. Subosits and J. C. Gerdes, "From the racetrack to the road: Real-time trajectory replanning for autonomous driving," *IEEE Transactions on Intelligent Vehicles*, vol. 4, no. 2, pp. 309–320, 2019.
- [4] A. Wischnewski, T. Herrmann, F. Werner, and B. Lohmann, "A tube-MPC approach to autonomous multi-vehicle racing on high-speed ovals," *IEEE Transactions on Intelligent Vehicles*, vol. 8, no. 1, pp. 368–378, 2023.
- [5] A. Liniger, A. Domahidi, and M. Morari, "Optimization-based autonomous racing of 1:43 scale RC cars," *Optimal Control Applications and Methods*, vol. 36, no. 5, pp. 628–647, 2014.
- [6] J. Dallas, M. Thompson, J. Goh, and A. Balachandran, "A hierarchical adaptive nonlinear model predictive control approach for maximizing tire force usage in autonomous vehicles," *Journal of Field Robotics*, vol. 3, no. 1, pp. 222–242, 2023.
- [7] T. P. Weber, R. K. Aggarwal, and J. C. Gerdes, "Human-inspired autonomous racing in low friction environments," *IEEE Transactions on Intelligent Vehicles*, pp. 1–14, 2024.
- [8] J. Kabzan, L. Hewing, A. Liniger, and M. N. Zeilinger, "Learning-based model predictive control for autonomous racing," *IEEE Robotics and Automation Letters*, vol. 4, no. 4, pp. 3363–3370, 2019.
- [9] A. Liniger, X. Zhang, P. Aeschbach, A. Georghiou, and J. Lygeros, "Racing miniature cars: Enhancing performance using stochastic MPC and disturbance feedback," in *American Control Conference*, 2017, pp. 5642–5647.
- [10] I. Mordatch, K. Lowrey, and E. Todorov, "Ensemble-CIO: Full-body dynamic motion planning that transfers to physical humanoids," in *IEEE/RSJ Int. Conf. on Intelligent Robots & Systems*, 2015.
- [11] I. Abraham, A. Handa, N. Ratliff, K. Lowrey, T. D. Murphy, and D. Fox, "Model-based generalization under parameter uncertainty using path integral control," *IEEE Robotics and Automation Letters*, 2020.
- [12] T. Brudigam, A. Capone, S. Hirche, D. Wollherr, and M. Leibold, "Gaussian process-based stochastic model predictive control for overtaking in autonomous racing," 2021, available at <https://arxiv.org/abs/2105.12236>.
- [13] R. Dyro, J. Harrison, A. Sharma, and M. Pavone, "Particle MPC for uncertain and learning-based control," in *IEEE/RSJ Int. Conf. on Intelligent Robots & Systems*, 2021.
- [14] T. Lew and M. Bonalli, R. Pavone, "Exact characterization of the convex hulls of reachable sets," in *Proc. IEEE Conf. on Decision and Control*, 2023.
- [15] M. Prajapat, A. Lahr, J. Köhler, A. Krause, and M. N. Zeilinger, "Towards safe and tractable Gaussian process-based MPC: Efficient sampling within a sequential quadratic programming framework," in *Proc. IEEE Conf. on Decision and Control*, 2024.
- [16] T. Lew, R. Bonalli, and M. Pavone, "Risk-averse trajectory optimization via sample average approximation," *IEEE Robotics and Automation Letters*, vol. 9, no. 2, pp. 1500–1507, 2024.
- [17] J. Y. Goh, T. Goel, and C. J. Gerdes, "Toward automated vehicle control beyond the stability limits: Drifting along a general path," *ASME Journal of Dynamic Systems, Measurement, and Control*, vol. 142, no. 2, 2019.
- [18] T. Kobayashi, T. P. Weber, and J. C. Gerdes, "Trajectory planning using tire thermodynamics for automated drifting," in *IEEE Intelligent Vehicles Symposium*, 2024.
- [19] E. Fiala, "Seitenkräften am rollenden luftreifen," *Vdl Zeitschrift*, vol. 96, pp. 973–979, 1954.
- [20] J. Svendenius, "Tire modeling and friction estimation," Ph.D. dissertation, Lund University, 2007.
- [21] A. Shapiro, D. Dentcheva, and A. Ruszczyński, *Lectures on Stochastic Programming: Modeling and Theory*, 2nd ed. Society for Industrial and Applied Mathematics, 2014.
- [22] S. P. Boyd and C. H. Barratt, *Linear controller design: limits of performance*. Citeseer, 1991, vol. 78.
- [23] R. Quirynen and K. Berntorp, "Uncertainty propagation by linear regression kalman filters for stochastic NMPC," *IFAC-Papers Online*, vol. 54, no. 6, pp. 76–82, 2021.
- [24] T. Lew, R. Bonalli, and M. Pavone, "Chance-constrained sequential convex programming for robust trajectory optimization," in *European Control Conference*, 2020.
- [25] C. Leparoux, R. Bonalli, B. Hérisse, and F. Jean, "Statistical linearization for robust motion planning," *Systems & Control Letters*, vol. 189, p. 105825, 2024.
- [26] J. Nocedal and S. J. Wright, *Numerical Optimization*, 2nd ed. Springer New York, 2006.
- [27] J. Bradbury, R. Frostig, P. Hawkins, M. J. Johnson, C. Leary, D. Maclaurin, G. Necula, A. Paszke, J. VanderPlas, S. Wanderman-Milne, and Q. Zhang, "JAX: composable transformations of Python+NumPy programs," 2018.
- [28] B. Stellato, G. Banjac, P. Goulart, A. Bemporad, and S. Boyd, "OSQP: an operator splitting solver for quadratic programs," *Mathematical Programming Computation*, vol. 12, no. 4, pp. 637–672, 2020.
- [29] M. Diehl, H. G. Bock, and J. P. Schlöder, "A real-time iteration scheme for nonlinear optimization in optimal feedback control," *SIAM Journal on Control and Optimization*, vol. 43, no. 5, pp. 1714–1736, 2005.
- [30] OxTS, "User manual: NCOM data format for the efficient communication of navigation measurements," 2022.
- [31] B. Plancher and S. Kuindersma, *A Performance Analysis of Parallel Differential Dynamic Programming on a GPU*, 2020.
- [32] M. Schubiger, G. Banjac, and J. Lygeros, "GPU acceleration of ADMM for large-scale quadratic programming," *Journal of Parallel and Distributed Computing*, vol. 144, pp. 55–67, 2020.
- [33] A. L. Bishop, J. Z. Zhang, S. Gurumurthy, K. Tracy, and Z. Manchester, "ReLU-QP: A GPU-accelerated quadratic programming solver for model-predictive control," in *Proc. IEEE Conf. on Robotics and Automation*, 2024.
- [34] E. Adabag, M. Atal, W. Gerard, and B. Plancher, "MPCGPU: Real-time nonlinear model predictive control through preconditioned conjugate gradient on the GPU," in *Proc. IEEE Conf. on Robotics and Automation*, 2024.